

NUV Star Catalog from the Lunar-based Ultraviolet Telescope Survey: First Release

Xian-Min Meng, Xu-Hui Han, Jian-Yan Wei, Jing Wang, Li Cao, Yu-Lei Qiu, Chao Wu, Jin-Song Deng, Hong-Bo Cai and Li-Ping Xin

Key Laboratory of Space Astronomy and Technology, National Astronomical Observatories, Chinese Academy of Sciences, Beijing 100012, China; mengxm@nao.cas.cn; hxx@nao.cas.cn

Received 2016 April 24; accepted 2016 June 29

Abstract We present a star catalog extracted from the Lunar-based Ultraviolet Telescope (LUT) survey program. LUT's observable sky area is a circular belt around the Moon's north pole, and the survey program covers a preferred area of about 2400 deg^2 which includes a region of the Galactic plane. The data are processed with an automatic pipeline which copes with stray light contamination, artificial sources, cosmic rays, flat field calibration, photometry and so on. In the first release version, the catalog provides high confidence sources which have been cross-identified with the Tycho-2 catalog. All the sources have signal-to-noise ratio larger than 5, and the corresponding magnitude limit is typically 14.4 mag, but can be as deep as ~ 16 mag if stray light contamination is at the lowest level. A total of 86 467 stars are recorded in the catalog. The full catalog in electronic form is available online.

Key words: Astronomical Databases: surveys — Astronomical Databases: catalogs — techniques: image processing — techniques: photometric — ultraviolet: stars

1 INTRODUCTION

The Lunar-based Ultraviolet Telescope (LUT) is the first robotic telescope deployed on the Moon's surface, and is mounted inside the lander of China's Chang'e-3 lunar exploration program (Ip et al. 2014). LUT and the lander are located at 44.12°N and 19.52°W on a basin of the Moon named Mare Imbrium (Sea of Showers). LUT is an imaging telescope working at a characteristic near-ultraviolet (NUV) band. Since the successful launch and landing of Chang'e-3 in December 2013, LUT finished the task of its one-year mission and it continued to work stably for another year. The stability of its performance has been verified by calibration work spanning 18 months of the zero point (zp). The photometric calibration gives $zp = 17.53 \pm 0.05$ mag, which is very consistent with the result from the first 6-months of $zp = 17.52 \pm 0.07$ mag (Wang et al. 2015a).

One of LUT's main scientific objectives is to conduct a sky survey over an area of about 2400 deg^2 (Cao et al. 2011). Tens of star catalogs covering NUV bands have already been published, which have been contributed by Galaxy Evolution Explorer (GALEX), Hubble Space Telescope (HST), etc. GALEX has an all sky survey project named All-Sky Imaging survey (AIS), whose detection limit is ~ 21 mag at an NUV band. GALEX avoids the Galactic plane during the prime mission phase because of safety limits related to high-count rate sources. Its latest

survey covers regions in the Galactic plane, but these data are not yet accessible in the public archive (Bianchi 2014). The LUT survey covers part of the low Galactic latitude region within its available sky area, so targeting this region would be helpful for future researches. Furthermore, the survey observation strategy used by LUT enables the telescope to revisit some sky areas more than 10 times, so it is potentially possible to find variable stars through further data mining.

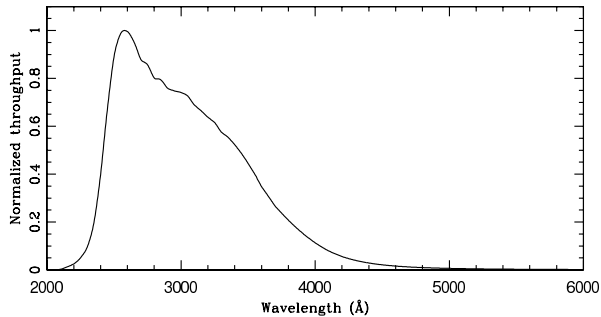
The LUT survey data are processed with an automatic pipeline, which is inherited from LUT's pointing observation data processing pipeline (see Meng et al. 2015). The main aspects of the survey program are: (1) data processing associated with the survey has to remove all cosmic rays, so it has to perform image stacking; (2) a series of processes have to be carried out to remove artificial sources that have arisen from stray light residuals.

The first release of the LUT survey data product, as described in this paper, is a star catalog covering all of LUT's available sky area, and is cross-identified with the optical star catalog Tycho-2 (Høg et al. 2000). Tycho-2 is the reference catalog for LUT's astrometry, and its positional and photometric data are very helpful for LUT to remove artificial sources.

After providing an overview of the LUT instrument in Section 2, the survey observation strategy and its footprint are described in Section 3. The details of the data process-

Table 1 Basic Parameters of LUT Instruments

Item	Value
Telescope aperture (mm)	150
Focal ratio	3.75
Field of view	$1.35^\circ \times 1.35^\circ$
CCD size (imaging area; pixel)	1024×1024
CCD pixel scale (arcsec/pixel)	4.76
Readout noise (e^-/pixel)	8
Dark current ($e^-/\text{pixel/s}$)	<0.2
Passband (nm)	245–345
Azimuth range of mirror rotation	$[-28^\circ, +13^\circ]$
Altitude range of mirror rotation	$[+20^\circ, +38^\circ]$

**Fig. 1** Normalized throughput curve of LUT system (Wang et al. 2015b).

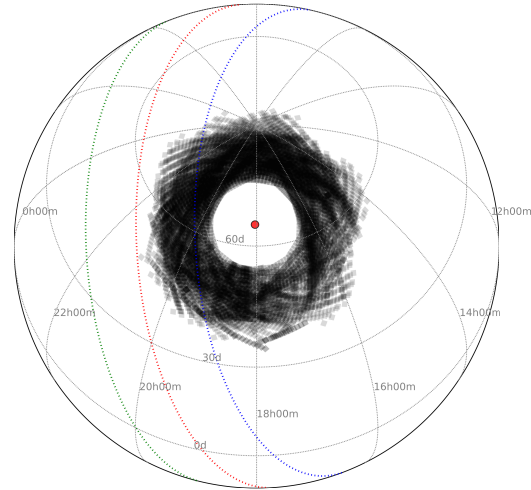
ing pipeline used by the survey are described in Section 4, and the performances in various aspects are also shown. A compilation of the catalog and some statistical results are presented in Section 5. A discussion on Galactic extinction and aperture correction is given in Section 6.

2 LUT INSTRUMENT

LUT is a Ritchey–Chrétien telescope working at a Nasmyth focus. A flat mirror is mounted on a two-dimensional gimbal in front of the telescope aperture for pointing and tracking (see Wang et al. 2015b, Fig. 1). An ultraviolet (UV)-enhanced back-illuminated AIMO CCD is mounted on the focal plane, and UV coating is applied on one lens of the field corrector as the UV filter. The final throughput of the LUT system has a peak value of $\sim 8\%$ at 2500 \AA . The throughput curve is shown in Figure 1. Two pairs of LEDs are installed crosswise (one as a backup) on the front inside wall of the camera, which is used to illuminate the CCD through a ring-like diffusion glass for flat field calibration. The LEDs emit at spectral wavelength 286 nm and the spectral width is $\sim 12 \text{ nm}$. Further details of the instrumentation and system performance are described by Cao et al. (2011) and Wang et al. (2015b). The basic parameters of the LUT instruments are listed in Table 1.

3 SURVEY OBSERVATIONS

LUT takes advantage of its own flat mirror and the Moon’s self-rotation to change the survey area of the sky, and hence has surveyed a wide circular belt around the Moon’s north

**Fig. 2** The LUT survey footprint, which covers $\sim 2400 \text{ deg}^2$. The red filled circle marks the position of lunar north pole in the epoch of 2015 Jan. 1; the black filled quadrangles mark individual sky coverage of LUT’s FOV at different times; the red dotted line marks the Galactic plane at $b = 0^\circ$; the blue and green dotted lines mark the Galactic latitudes of $b = +15^\circ$ and $b = -15^\circ$, respectively.

pole. This area is generally between latitude 60°N and 80°N in the Moon-fixed coordinate system¹, and the total survey area is $\sim 2400 \text{ deg}^2$. During each lunar daytime, LUT’s survey program may have 13 observation sequences which always contain 36 different pointings. The pointing directions are always shifted by 1° and overlap with each other, which is designed for the completeness of sky coverage. Each sky area was observed for 10 min with a single exposure time of 30 s and idle for 30 s (designed to meet the requirement defined by the total data size limit of Chang’e-3). During the observation of each sky area (10 min), the direction of pointing stays stationary relative to the Moon’s surface. In each lunar month the observation time of the survey program totals 72 hours. The observation time sequences of the pointings are calculated at each beginning of lunar daytime, and also a survey mosaic is simulated by a separately developed code.

The sky coverage of the LUT survey is illustrated in Figure 2. The red filled circle marks the position of the lunar north pole in the epoch of 2015 Jan. 1²; the black filled quadrangles mark individual sky coverage areas of LUT’s field of view (FOV) in J2000 coordinates at differ-

¹ The origin is the barycenter of the Moon; the z -axis coincides with the mean rotational axis (pole) of the Moon; the zero latitude circle is the equatorial plane; the prime meridian (0° longitude) is defined by the mean Earth direction (Qi et al. 2015).

² Calculated through the IAU Working Group on Cartographic Coordinates and Rotational Elements (WGCCRE) report (Archinal et al. 2011).

ent times; the red dotted line marks the Galactic plane at $b = 0^\circ$; the blue and green dotted lines mark Galactic latitudes of $b = +15^\circ$ and $b = -15^\circ$, respectively. Figure 2 shows that a part of the low Galactic latitude ($b < 15^\circ$) region is covered by the LUT survey, which provides valuable measurement of stars in this region at the NUV band.

4 DATA PROCESSING FOR THE SURVEY PROGRAM

The survey data processing pipeline is an automatic system. It is inherited from the pipeline of LUT’s pointing observation programs (Meng et al. 2015), so the main strategy, algorithms and many procedures are similar to the latter. It starts from each raw image, and results in producing a star catalog of each specified sky area. The outline of the pipeline is listed in Table 4. In this section, the procedures that are similar to the pointing programs will be shortly covered first, and the extra parts of the survey pipeline will be described in detail in the following subsections.

Observations with LUT suffer from stray light contamination caused by sunlight being scattered by the cabin and the telescope. The pattern of stray light can be removed by subtracting a stray light template generated from the observation images. After being grouped according to their pointing directions and observation times, the images are combined with a “median” algorithm to produce stray light templates. Because the flat mirror stays stationary during each pointing period and the Moon’s self-rotation leads to little offsets (~ 4 pixel) of the source positions between adjacent exposures, combining images can produce stray light templates without any point sources. Then, stray light can be removed by subtracting the template from the original images. Bias and dark current are also subtracted along with the stray light pattern.

Flat field images are produced by making use of dithering observations. We use internal LED lamps to produce flat images which will be flattened to correct pixel-to-pixel relative nonuniformity, and employ dithering observation of individual standard stars to sample the large-scale nonuniformity in the FOV. So, the flat fielding correction is accomplished in two steps, a pixel-to-pixel flat fielding and a large-scale flat fielding using an image produced by 2-D surface fitting to the sampled fluxes of the calibration star.

After image stacking (Sect. 4.1) and astrometry calibration (Sect. 4.2), source candidates are extracted from each stacked image by SExtractor (Bertin & Arnouts 1996). Some criteria are adopted to exclude abnormal or irrelative source candidates for subsequent procedures. The first step is to clean the candidates which (1) are in the margin regions of the images; (2) have negative fluxes measured by SExtractor; (3) have $\text{ELONGATION} > 3$ (major-axis/minor-axis > 3); (4) have photometry failure flags; (5) have abnormal background values, and (6) have $\text{FWHM}_s < 1.3$ pix or $\text{FWHM}_s > 4$ pix, according to the distribution of FWHMs which peaks at 2 pix and extends to 3.5 pix. The other step is performed after aperture photom-

etry, and its purpose is to remove artificial sources that arise from residual stray light (see Sect. 4.4).

A typical value of FWHM is determined for a group of images as the unit of aperture radius for photometry. The typical FWHM of each group is denoted as FWHM_{med} . The method to determine FWHM_{med} is described by Meng et al. (2015). When aperture photometry and PSF photometry (see Sect. 4.3) are finished, a star catalog recording all the output results is generated for every image. These catalogs are merged to generate the preliminary source catalog of LUT.

The data processing procedures that are different from the pointing program are described in the following subsections.

4.1 Image Stacking

The image stacking procedure combines the images by computing the “median” value of every pixel. The main purposes of the image stacking procedure are: (1) to remove cosmic rays; (2) to increase detection depth and signal-to-noise ratio (SNR); (3) to solve the charge transfer efficiency (CTE) problem. The CTE problem is found on the CCD used by LUT where residual charges may be left after the readout. This may happen after some types of cosmic ray strikes, and disappear after one more exposure. Therefore, to filter out cosmic rays and their residual charges, the number of coadded images should not be less than 5, and typically, the number is set to be 8, because this is the typical total number of images for each survey patch observation.

Before applying the “median” image stacking, the images are grouped according to their pointing directions, and the time duration of a group is restricted to be within 10 min. Then, the images of each group are aligned according to the physical positions of the point sources on the images. Finally, the “median” image stacking is performed.

4.2 Astrometry

The astrometry procedure for the survey images follows the same procedure in the pointing program (Meng et al. 2015). In short, after converting the epoch of the Tycho-2 catalog to the current time and correcting the positions of Tycho-2 stars for proper motion, the geometrical distribution of 5–10 bright stars on an LUT image are matched with the Tycho-2 catalog.

In addition to cross matching their positions, their brightnesses are used as another cross-matched criterion to exclude false matching which could correlate two unrelated stars. The International Celestial Reference System (ICRS) at epoch J2000 is adopted for the astrometry result whose precision is typically about $1''$ (for the stars that are used in astrometry).

Table 2 Outline Of Survey Data Processing Pipeline To Produce Level-2 Data

Outline of Survey Data Processing Pipeline	
0. Data preparation	
1. Overscan correction and imaging area trimming	
<i>Stray Light Removal</i>	
2. Image grouping according to pointing direction and time period	
3. Image combination to produce stray light pattern template	
4. Each image subtracts its stray light template	
5. Flat fielding making use of dithering observation	
6. Image stacking	
7. Astrometry	
8. Source Extraction	
<i>Profile Measurement and Source Cleaning (1st Cleaning)</i>	
9. Remove abnormal objects which are at the edges of images or have negative fluxes, ELONGATION>3, etc.	
10. Measure full width at half maximums (FWHMs) of the Moffat profile and keep objects which have $1.3 < \text{FWHM} < 4$	
11. Determine typical FWHM for an image group and assign to FWHM_{med}	
<i>Photometry</i>	
12. Aperture photometry	
13. Cleaning artificial sources (2nd cleaning) through a cluster analysis method	
14. PSF photometry	
15. Catalogs archiving	

Table 3 Catalog Format

Column Header	Units	Description
LUTID	—	LUT object identifier
RA_LUT	degree	Right ascension in LUT records, ICRS, epoch = J2000
DEC_LUT	degree	Declination in LUT records, ICRS, epoch = J2000
FWHM	pix	FWHM of the star, measured by PYRAF.PSFMEASURE code
R_AP	pix	Aperture radius used for aperture photometry
MAG_LUT	mag	Magnitude at LUT band measured with $2 \times \text{FWHM}$ aperture radius
MERR_LUT	mag	Uncertainty of MAG_LUT
PSF_LUT	mag	Magnitude measured through PSF modeling
PSF_ERR	mag	Uncertainty of PSF_LUT
JD	d	Julian date of UT time associated with LUT observation
TYCHOID	—	Tycho-2 identifier
RA_TYC	degree	Right ascension in Tycho-2 records, ICRS, epoch = J2000
DEC_TYC	degree	Declination in Tycho-2 records, ICRS, epoch = J2000
BTMAG	mag	Tycho-2 B_T magnitude
VTMAG	mag	Tycho-2 V_T magnitude
SEPARATION	arcsec	Separation distance of the positions between LUT and Tycho-2

4.3 Photometry

LUT photometries adopt the AB magnitude system defined by Oke & Gunn (1983) and the magnitudes are obtained as

$$m_{\text{LUT}} = m_{0,\text{LUT}} - 2.5 \log f_{\text{LUT}}, \quad (1)$$

where $m_{0,\text{LUT}}$ is the magnitude zero point of LUT and f_{LUT} is the flux density in the unit of $\text{ergs s}^{-1} \text{cm}^{-2} \text{Hz}^{-1}$. The zero point of LUT is determined from observations of standard stars provided by the International Ultraviolet Explorer (IUE) mission (Wu et al. 1998). The theoretical spectra of these standards were extracted from the ATLAS9 stellar atmosphere models (Castelli & Kurucz 2003) and their absolute fluxes were determined according to their V -band magnitudes recorded in the SIMBAD database. After constructing theoretical spectra for the

standards, the expected magnitude of star i , $m_{i,\text{exp}}$ in the LUT system, was calculated by utilizing the pre-determined throughput curve of LUT. With an arbitrary magnitude zero point $m_{0,\text{inst}}$, the instrumental magnitude of star i was measured to be $m_{i,\text{inst}}$, and so the zero point of LUT can be calculated through $m_{0,\text{LUT}} = m_{0,\text{inst}} - (m_{i,\text{inst}} - m_{i,\text{exp}})$. The statistical result of all the calibration stars observed at different times gives the final magnitude zero point of LUT as $m_{0,\text{LUT}} = 17.52 \pm 0.05$, and this value remains stable in an 18-month operational performance test. For details of the LUT photometry calibration and stability of the zero point over 18 months please refer to Wang et al. (2015b) and Wang et al. (2015a).

Aperture photometries are performed with an aperture radius of $2 \times \text{FWHM}_{\text{med}}$, where FWHM_{med} represents the typical FWHM of stars. The background

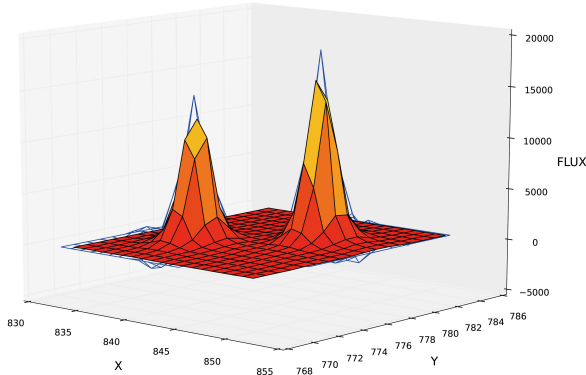


Fig. 3 PSF modeling for a double star 16 Cyg.

annulus for aperture photometry adopts $6 \times \text{FWHM}_{\text{med}}$ and $9 \times \text{FWHM}_{\text{med}}$ as inner and outer radii, respectively. Aperture photometries are performed by the PYRAF.APPHOT.PHOT code. SNR is calculated as

$$\text{SNR} = \frac{F}{\sqrt{\frac{F}{G} + A \times \sigma^2 + \frac{A^2 \times \sigma^2}{N_{\text{sky}}}}}, \quad (2)$$

where F is the total number of counts excluding the background in the aperture, G is the gain of the CCD (electrons per ADU), A is the area of the aperture, σ is the standard deviation of the background, and N_{sky} is the pixel count of the background. The uncertainty in aperture photometry is calculated as $m_{\text{err,LUT}} = 1.0857/\text{SNR}$ and is typically $m_{\text{err,LUT}} \sim 0.006$ mag for a star of $m_{\text{LUT}} = 10$ mag (30 s exposure). It rises to about 0.2 mag at magnitude ~ 14.4 which is the 5σ detection.

PSF photometries are also performed to provide more reliable measurements for crowded stars. The pipeline has been tested to have the capability to extract positions of contacting and crowded stars, and to model their PSF profiles. The actual effect of the PSF photometry for a double star 16 Cyg is illustrated in Figure 3.

4.4 Removing Artificial Sources

The procedure for removing stray light sometimes leaves a residual pattern on the resulting images if stray light varies with time and the current strategy cannot totally remove stray light. Stray light residuals may cause source extraction to give false sources, which are actually noises from the residuals. To identify such false sources, we employ cluster analysis in a 2-D parameter space. The background values of sources “MSKY” and the standard deviations “STDEV” of “MSKY” are used for clustering. The machine learning package SCIKIT-LEARN (Pedregosa et al. 2011) and its DBSCAN clustering method are used for this task. Real celestial objects are selected as the cluster located within a region which is the closest to (0,0) in

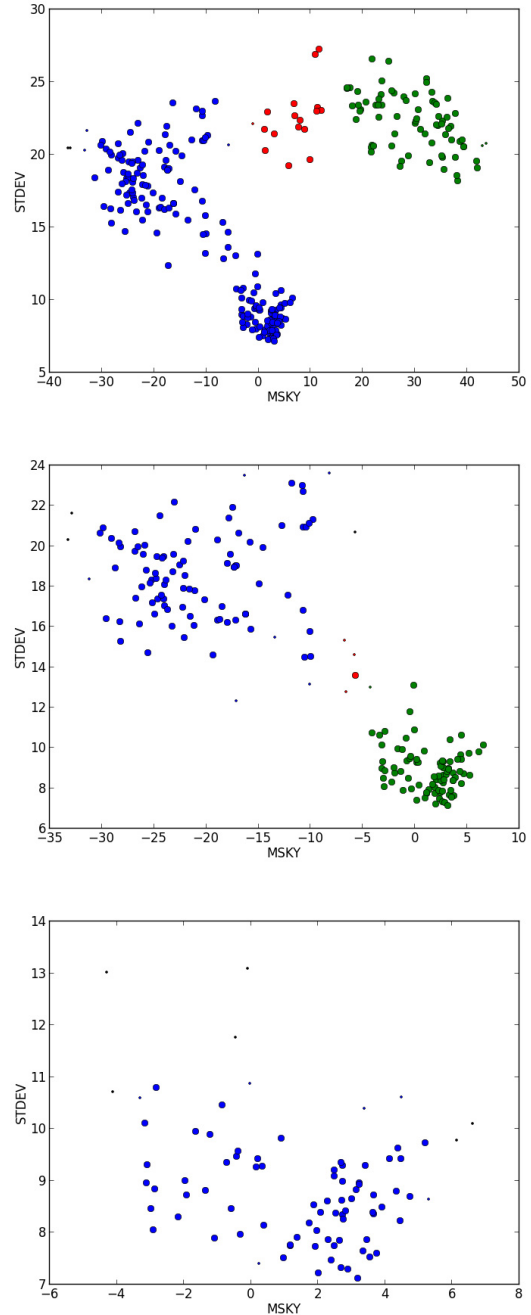


Fig. 4 An example of the three-step iteration of cluster analysis in MSKY–STDEV space, where “MSKY” is the source’s background value and “STDEV” is the standard deviation of “MSKY.” The colors mark different clusters divided in each iteration step of cluster analysis. Smaller circles are non-core samples that are still part of a cluster, and black points mark the outliers.

the MSKY–STDEV space³. Based on experimentation, the range of this region should be smaller than 5×8 . The clus-

³ “MSKY” should be close to 0 because the background has been subtracted along with stray light; “STDEV” is required to be the smallest where the noise of the background is the lowest.

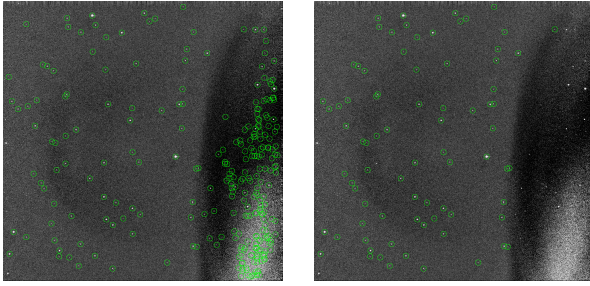


Fig. 5 The effect of cleaning artificial sources. In the left panel, there are residuals from removal of stray light on the right side and they lead to extraction of artificial sources. After the procedure to remove artificial sources is applied, most of them are filtered out as shown in the right panel .

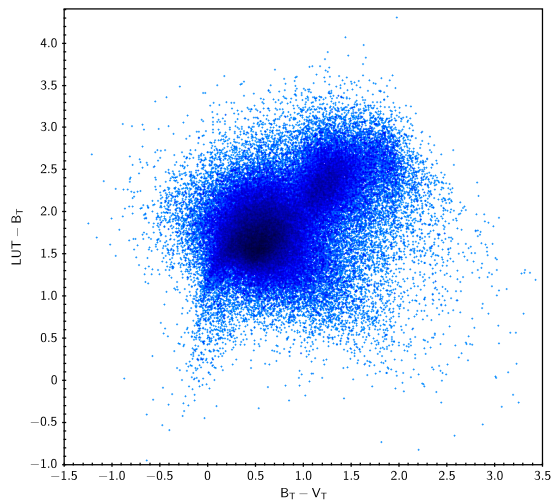


Fig. 6 A color-color diagram of $LUT - B_T$ vs. $B_T - V_T$ associated with the catalog.

ter analysis for each image is performed with no more than three iterations.

Figure 4 shows an example of a three-step iteration, and its result is illustrated in the right panel of Figure 5, in which the artificial objects in the left panel have been removed. Furthermore, an SNR cut is applied to select high confidence detections, which have $SNR \geq 5$, since false sources always have lower SNR.

5 THE CATALOG

In the first released version of the LUT survey catalog, we provide high confidence sources with $SNR \geq 5$, and sources that have been cross matched with the Tycho-2 catalog (Høg et al. 2000). The catalog with 86 467 lines is available as catalog I/335 from CDS⁴ (the Strasbourg astronomical Data Center).

⁴ <http://cdsarc.u-strasbg.fr/viz-bin/Cat?cat=I/335>

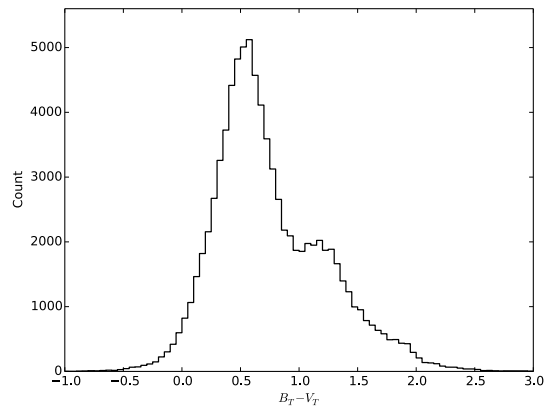
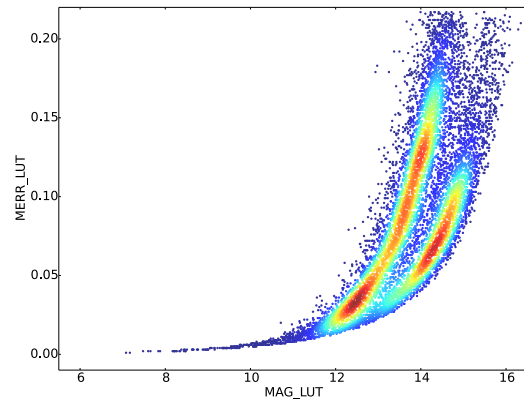
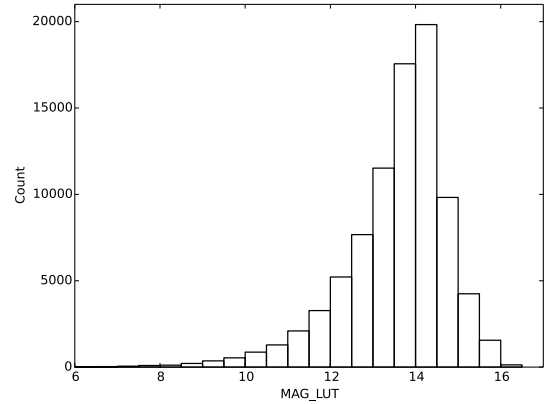


Fig. 7 Some statistical properties of the catalog. *Top*: Magnitude distribution of stars in the catalog; *middle*: the relation between the brightnesses and photometric accuracies, in which red indicates the densest region; there are two tracks in the relation because the right track was obtained when stray light contamination is much smaller; *bottom*: distribution of stars' spectral types.

5.1 Catalog Compilation

The first step in catalog construction is to deal with multiple observations of the sources, which have been revisited by the survey many times and have several records in the catalog. The representative record of each source is se-

lected to be the first one in the primitive catalog. This step generates $\sim 158\,354$ individual sources observed by LUT.

The second step is to positionally cross-match the LUT catalog with the Tycho-2 catalog. The purpose of this step is to identify the LUT stars in the established databases. The cross matching is initially performed finding the nearest counterparts between the two catalogs within $10''$, i.e. nearly two pixels as separation distance. The distribution of the separation distance shows that more than 99% of the resultant sources have been included within $4''$, which is slightly less than the pixel scale of $4.76''$ for LUT. So, we adopt $4''$ as the criterion for positional matching. This criterion results in a total number of 86 467 entries for the final catalog. Proper motions of the stars were not considered, because such factors between epoch J2000 and the current time are negligible compared to the cross-matching distance of $4''$. The result of cross matching can be examined by a color-color diagram in Figure 6. The dense region near $LUT-B_T \sim 1.5$ mag is typical for $B_T - V_T \sim 0.5$ mag stars (F and G type), which is consistent with the theoretical estimation performed by Han et al. (2016, in preparation). The number density drops to around $LUT-B_T = 2.0$ mag, which is consistent with the 5σ detections of LUT’s 14.4 mag and Tycho-2’s $B_T \sim 12.5$ mag.

5.2 Catalog Format

The catalog provides data from the LUT survey and the corresponding Tycho-2 records. Table 3 describes the format of the catalog.

5.3 Statistics

Some statistical properties of the catalog are shown in Figure 7. The top panel of Figure 7 shows the histogram of the LUT band magnitude. The majority of the sources in the catalog have brightness of 13–15 mag at the NUV band. The faint end extends down to ~ 16 mag, whose corresponding sources were observed at the early times of each lunar daytime when stray light was at the lowest level.

Typical photometric accuracies can be derived from the middle panel of Figure 7. The diagram displays the relation between aperture photometry uncertainties and brightness. The plot gives a typical uncertainty of 0.2 mag at magnitude ~ 14.4 , so we define 14.4 mag as the 5σ detection limit of the LUT survey program.

The distribution of spectral types can be found in the bottom panel of Figure 7. The peak of the distribution occurs at $B_T - V_T = 0.5 - 0.6$ mag, where F and G type stars may dominate. A minor peak can be found around $B_T - V_T = 1.2$ mag, which K and M type stars may have.

6 DISCUSSION

6.1 Extinction

The photometric results in the catalog are not corrected for Galactic extinction. The reasons are:

- (1) The sources are in principle stars in the Milky Way and extinction correction for Galactic sources is complicated. At least, we need to have information on their distances, but actually they are lacking.
- (2) The uncertainty in the correction should be significant. First, even if we had their distance information, their associated dust/gas amounts are hard to estimate; Second, for example, a certain method of Galactic dust reddening estimation may have an uncertainty of about 16% (Schlegel et al. 1998), which may be much larger than the uncertainty in the photometry results.
- (3) The extinction correction may introduce errors to photometric results, and these are systematic errors which come from the correction factors and should be treated differently from random errors.

6.2 Aperture Correction

The catalog does not include aperture corrections for photometry results. We give the correction factor separately in this section as a choice that is subject to the users. The reason is as follows. Because of the image stacking, the form of the brightness profile of stars may vary in a considerable range, depending on the precision of the image alignment, variation of profiles between single-exposures, field distortion, etc. Therefore, the aperture effect of the survey data photometry is a complicated problem. The aperture correction method for survey data is associated with the pointing observation (see Meng et al. 2015, Sect. 4). We measured the “curve of growth” for 26 bright stars in different survey images and their physical positions were varying. The scatter of the growth curves from the survey program is obviously larger than that of the pointing program, and their profiles are different (see the median stacked profiles shown in Fig. 8). Therefore, the uncertainty in the aperture correction factor for the survey program is larger than that for the pointing program.

As derived from the growth curve, the aperture correction factor for a $2 \times \text{FWHM}$ aperture radius is $\Delta m_{r_2} = -0.029 \pm 0.011$, if the aperture correction is performed with

$$m_{r_2, \text{cor}} = m_{r_2} + \Delta m_{r_2}, \quad (3)$$

where m_{r_2} and $m_{r_2, \text{cor}}$ are the magnitudes before and after aperture correction, respectively.

7 SUMMARY

A star catalog obtained from the observation data of the LUT survey program is presented here, which has 86 467 entries of stars at the NUV band. The sky coverage of the catalog is about 2400 deg^2 , a circular belt around the Moon’s north pole, and a part of it has low Galactic latitude of $b < 15^\circ$. An automatic pipeline is developed to process the data, coping with stray light contamination and thereby false sources, cosmic rays, flat field calibrations, photometries, etc. In this first released version, the catalog provides high confidence sources that have been

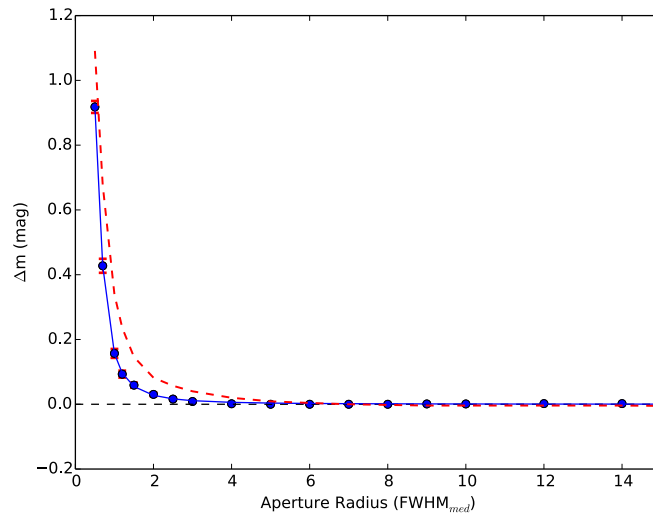


Fig. 8 The curve of growth and its dispersions of combined LUT images of the survey data (blue circles and red error bars). The blue solid line is a Voigt model fitting to the curve of growth. The red dashed line representing the curve of growth for LUT single-exposure images, as has described by Meng et al. (2015), is shown here for comparison.

cross-identified with the Tycho-2 catalog. The SNR is constrained to be ≥ 5 , and the corresponding detection limit of the LUT survey is about 14.4 mag. Some statistical properties are given here. The full catalog in electronic form is available as catalog I/335 from CDS.

Acknowledgements This project is supported by the Key Research Program of Chinese Academy of Sciences (KGED-EW-603), the National Basic Research Program of China (973-program, Grant No. 2014CB845800) and the National Natural Science Foundation of China (Grant Nos. 11203033, 11473036, U1231115 and U1431108). This project made use of SExtractor, a powerful program for astronomical data analysis; ASTROPY, a community-developed core PYTHON package for astronomy (Astropy Collaboration, 2013); MATPLOTLIB, a 2D graphics package for PYTHON (Hunter 2007); PYRAF and PYFITS, products of the Space Telescope Science Institute, which is operated by AURA for NASA; and the SIMBAD database, operated at CDS, Strasbourg, France. This project makes a lot of use of the tabular data analysis and visualization software TOPCAT (Taylor 2005) to do archiving works, which has not been described in the text.

References

- Archinal, B. A., A'Hearn, M. F., Bowell, E., et al. 2011, *Celestial Mechanics and Dynamical Astronomy*, 109, 101
- Bertin, E., & Arnouts, S. 1996, *A&AS*, 117, 393
- Bianchi, L. 2014, *Ap&SS*, 354, 103
- Cao, L., Ruan, P., Cai, H., et al. 2011, *Science China Physics, Mechanics, and Astronomy*, 54, 558
- Castelli, F., & Kurucz, R. L. 2003, in *IAU Symposium*, 210, *Modelling of Stellar Atmospheres*, eds. N. Piskunov, W. W. Weiss, & D. F. Gray, 20P
- Høg, E., Fabricius, C., Makarov, V. V., et al. 2000, *A&A*, 355, L27
- Hunter, J. D. 2007, *Computing in Science and Engineering*, 9, 90
- Ip, W.-H., Yan, J., Li, C.-L., & Ouyang, Z.-Y. 2014, *RAA (Research in Astronomy and Astrophysics)*, 14, 1511
- Meng, X.-M., Cao, L., Qiu, Y.-L., et al. 2015, *Ap&SS*, 358, 24
- Oke, J. B., & Gunn, J. E. 1983, *ApJ*, 266, 713
- Pedregosa, F., Varoquaux, G., Gramfort, A., et al. 2011, *Journal of Machine Learning Research*, 12, 2825 (arXiv:1201.0490)
- Qi, Z., Yu, Y., Cao, L., et al. 2015, *PASP*, 127, 1152
- Schlegel, D. J., Finkbeiner, D. P., & Davis, M. 1998, *ApJ*, 500, 525
- Taylor, M. B. 2005, in *Astronomical Society of the Pacific Conference Series*, 347, *Astronomical Data Analysis Software and Systems XIV*, eds. P. Shopbell, M. Britton, & R. Ebert, 29
- Wang, J., Meng, X. M., Han, X. H., et al. 2015a, *Ap&SS*, 360, 10
- Wang, J., Cao, L., Meng, X.-M., et al. 2015b, *RAA (Research in Astronomy and Astrophysics)*, 15, 1068
- Wu, C., Mo, J., Crenshaw, D. M., & Schiffer, F. H. 1998, in *ESA Special Publication*, 413, *Ultraviolet Astrophysics Beyond the IUE Final Archive*, eds. W. Wamsteker, R. Gonzalez Riestra, & B. Harris, 751